

Monte Carlo investigation of phase transitions and an incommensurate phase in Rb_2ZnCl_4 crystals

N. G. Zamkova and V. I. Zinenko

Institute of Physics, Siberian Branch of the Russian Academy of Sciences, 660036 Krasnoyarsk, Russia

(Submitted 18 November 1994)

Zh. Éksp. Teor. Fiz. **107**, 1282–1297 (April 1995)

The order-disorder model is used to investigate successive phase transitions and an incommensurate phase in a Rb_2ZnCl_4 crystals. The effective interaction constants between the ordered ZnCl_4 tetrahedra are calculated on the basis of an electrostatic model. It is found that these constants fluctuate as a function of distance in both sign and magnitude. There is, therefore, a strong competition between the interactions. The phase diagram and thermodynamic properties of the model are investigated by the Monte Carlo method. The calculations were performed for $12 \times 12 \times 24$ and $16 \times 16 \times 24$ lattices using two types of boundary conditions. A succession of structural phase transitions, including an intermediate modulated phase, which exists in the experimental temperature range, is obtained. The structure of the incommensurate phase is found to contain, besides long-wavelength modulation along the pseudo-hexagonal axis, a short-wavelength modulation with a period equal to that of the low-temperature ferroelectric phase. The computed temperature dependence of the specific heat, spontaneous polarization, and intensity of the satellite reflections in the modulated phase agrees satisfactorily with the experimental data for Rb_2ZnCl_4 crystals. © 1995 American Institute of Physics.

1. INTRODUCTION

Rubidium tetrachlorozincate Rb_2ZnCl_4 belongs to a large family of crystals with the general formula ACBX_4 , where A and C are alkali metals and BX_4 is a tetrahedral group (SO_4 , SeO_4 , CrO_4 , ZnCl_4 , and so on). This family of crystals has been attracting the attention of investigators for many decades. These substances are of interest because a great diversity of successive structural phase transitions with unusual physical properties depending on the chemical composition and the external conditions is observed in them. Incommensurate phases have been discovered in some members of this family of crystals. These phases are of interest from the standpoint of fundamental solid-state physics. A large number of experimental investigations of ACBX_4 compounds have been performed; information about the structures, phase diagrams, and physical properties of these materials can be found in Ref. 1, the reviews Refs. 2 and 3, and the literature cited in these works.

It is important to underscore the fact that all currently known structures of these compounds have one property in common. Specifically, they are all derivatives of the high-symmetry hexagonal phase with the space group $P6_3/mmm (D_{6h}^4)$. In some compounds, this phase is observed at high temperatures. However, indications of a hexagonal phase are observed in, for example, the domain structure up to the melting or decomposition temperature even in crystals with structures of lower symmetry. The distortions in the low-symmetry phases are mainly associated with the rotation of the tetrahedral groups with respect to both one another and the crystallographic axes of the hexagonal phase.^{1–3} An important feature of the hexagonal phase of these substances is that the BX_4 tetrahedra in it are necessarily disordered with respect to several equilibrium positions,

and it is therefore natural to conjecture that the observed distorted structures are a result of phase transitions associated with uniform and (or) nonuniform ordering of these groups.

At high temperatures Rb_2ZnCl_4 has a $\beta\text{-K}_2\text{SO}_4$ structure (*P* phase) and four molecules in an orthorhombic unit cell (space group *Pnam*). At 302 K it undergoes a phase transition into an incommensurate phase with modulation vector $\mathbf{q} = (1 - \delta)\mathbf{c}^*/3$, where \mathbf{c}^* is the first reciprocal-lattice vector in the hexagonal direction. As the crystal cools further, δ decreases and vanishes at 189 K when the system is locked into the ferroelectric commensurate phase (*F* phase, space group *Pna2*₁), in which the pseudo-hexagonal axis is tripled compared to the room-temperature phase, so that the unit cell contains twelve molecules. With further cooling Rb_2ZnCl_4 undergoes another transition at 74 K into a monoclinic phase, whose space group has still not been determined. These phase transitions are undergoing intensive experimental study (see Refs. 1–3 and references cited there). The phase transitions in Rb_2ZnCl_4 have been described theoretically both from the phenomenological and microscopic viewpoints.^{1,2,4}

The static structures of the *P* and *F* phases, the dynamic states of Rb_2ZnCl_4 at different temperatures in the *P* phase, and transitions from the paraelectric into the ferroelectric phase and from the ferroelectric into the monoclinic phase at low temperatures were studied in Ref. 4 by the method of molecular dynamics. The inter- and intramolecular interactions were calculated by means of an *ab initio* quantum-chemical approach. However, the structure of the incommensurate phase (*I*), the phase transitions $P \rightarrow I \rightarrow F$, and the behavior of the thermodynamic properties of Rb_2ZnCl_4 near the transitions were discussed in Ref. 4.

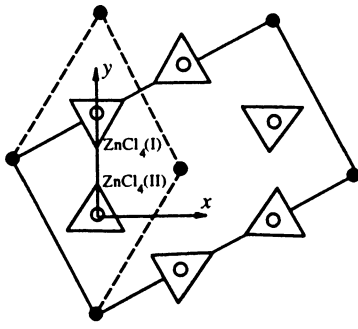


FIG. 1. Projection of the average structure of Rb_2ZnCl_4 on a plane perpendicular to the hexagonal axis in the D_{6h}^3 phase.

In the present work phase transitions in Rb_2ZnCl_4 are investigated using an approach that is based on the assumption that Rb_2ZnCl_4 , like other crystals of the ACBX_4 family, has an hexagonal paraphase with the space group $P6_3/mmm$ and that the observed sequence of phase transitions is associated with ordering of the BX_4 tetrahedra, which in this phase have four equally probable positions of equilibrium.^{5,6}

In Sec. 2 the effective interaction constants between the ordered tetrahedra are calculated on the basis of the electrostatic model. It is shown that the sign and magnitude of these constants fluctuate as function of the distance, as a result of which there is a strong competition between the interactions. It is well known that mean-field approximations are not suitable for investigating the thermodynamic properties of systems with competing interactions. For this reason we employ the Monte Carlo method, which is described in Sec. 3, to calculate the phase diagram and the thermodynamics of the phase transitions. The computational results are presented in Sec. 4. The phase diagram of Rb_2ZnCl_4 with an intermediate modulated phase is obtained, the temperature dependence of the modulation vector is calculated, and the thermodynamic characteristics of the phase transitions are calculated. In Sec. 5 the results are discussed and compared to existing experimental data.

2. THE MODEL. CALCULATION OF THE INTERACTION CONSTANTS

The projection of the structure of the hexagonal phase of Rb_2ZnCl_4 is shown in Fig. 1. To calculate the effective interaction constants and the thermodynamic properties we employ the model proposed in Ref. 5. In this model it is assumed that in the hexagonal phase the BX_4 tetrahedra are disordered with respect to the four equilibrium positions (Fig. 2). The interaction constants are calculated on the basis of the electrostatic model.⁷

We start from the Hamiltonian

$$H = -\frac{1}{2} \sum \mathbf{V}_{oo}^{I,I}(\mathbf{r}-\mathbf{r}') C_i^I(\mathbf{r}) C_j^I(\mathbf{r}') - \frac{1}{2} \sum \mathbf{V}_{oo}^{II,II}(\mathbf{r}-\mathbf{r}') C_i^{II}(\mathbf{r}) C_j^{II}(\mathbf{r}')$$

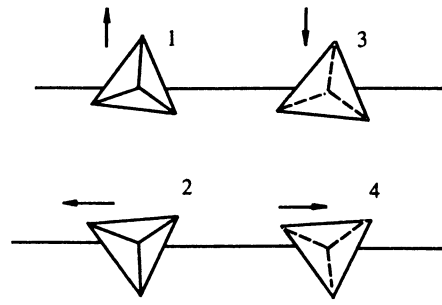


FIG. 2. Four positions of the ZnCl_4 tetrahedra in the D_{6h}^4 phase.

$$\begin{aligned} & - \sum \mathbf{V}_{oo}^{I,II}(\mathbf{r}-\mathbf{r}') C_i^I(\mathbf{r}) C_j^{II}(\mathbf{r}') + \sum \mathbf{F}_{od}^{IA}(\mathbf{r}-\mathbf{r}') C_i^I(\mathbf{r}) \mathbf{d}_A(\mathbf{r}') \\ & + \sum \mathbf{F}_{od}^{IC}(\mathbf{r}-\mathbf{r}') C_i^I(\mathbf{r}) \mathbf{d}_C(\mathbf{r}') + \sum \mathbf{F}_{od}^{IIA}(\mathbf{r}-\mathbf{r}') C_i^{II}(\mathbf{r}) \mathbf{d}_A(\mathbf{r}') \\ & + \sum \mathbf{F}_{od}^{IIC}(\mathbf{r}-\mathbf{r}') C_i^{II}(\mathbf{r}) \mathbf{d}_C(\mathbf{r}') + \frac{1}{2\alpha_A} \sum d_A^2(\mathbf{r}) \\ & + \frac{1}{2\alpha_C} \sum d_C^2(\mathbf{r}) \\ & + \frac{1}{2} \sum D_{\alpha\beta}^A(\mathbf{r}-\mathbf{r}') d_\alpha^A(\mathbf{r}) d_\beta^A(\mathbf{r}') + \frac{1}{2} \sum D_{\alpha\beta}^C(\mathbf{r}-\mathbf{r}') d_\alpha^C(\mathbf{r}) d_\beta^C(\mathbf{r}') + \sum D_{\alpha\beta}^{AC}(\mathbf{r}-\mathbf{r}') d_\alpha^A(\mathbf{r}) d_\beta^C(\mathbf{r}'), \end{aligned} \quad (1)$$

where

$$C_i^{I,II} = \begin{cases} 1, & \text{if the } \text{BX}_4 \text{ group occupies position } i \\ 0, & \text{otherwise.} \end{cases}$$

The equation (1) takes into account the fact that the unit cell in the hexagonal phase contains two nonequivalent tetrahedra (two ordered sublattices) which we distinguish by the indices I and II. In Eq. (1) the matrix $\mathbf{V}_{oo}(\mathbf{r}-\mathbf{r}')$ represents the direct octupole–octupole interaction between tetrahedra, which are assumed to be regular; $\mathbf{d}_{A,C}$ are the dipole moments of metals of the type A(Rb_2) and C(Rb_1) and are assumed to be point dipoles with polarizabilities α_A and α_C . We note that in the present calculation the polarizabilities of the metals Rb_1 and Rb_2 are adjustable parameters, since, together with the electronic polarizability, they also take into account the elastic polarizability associated with the displacement of the metal ions. The matrix $\mathbf{D}^{A,C}(\mathbf{r}-\mathbf{r}')$ represents the dipole–dipole interaction matrix between the metals and the matrix $\mathbf{F}_{od}(\mathbf{r}-\mathbf{r}')$ represents the octupole–dipole interaction. The effective Hamiltonian is obtained from Eqs. (1) by the standard transformations:⁸

$$\mathbf{H}_{\text{eff}} = -\frac{1}{2} \sum \mathbf{V}_{ij}^{\text{II}}(\mathbf{r}-\mathbf{r}') C_i^{\text{I}}(\mathbf{r}) C_j^{\text{I}}(\mathbf{r}') - \frac{1}{2} \sum \mathbf{V}_{ij}^{\text{II}}(\mathbf{r}-\mathbf{r}') C_i^{\text{II}}(\mathbf{r}) C_j^{\text{II}}(\mathbf{r}') - \sum \mathbf{V}_{ij}^{\text{II}}(\mathbf{r}-\mathbf{r}') C_i^{\text{I}}(\mathbf{r}) C_j^{\text{II}}(\mathbf{r}'), \quad (2)$$

where

$$\mathbf{V}_{ij}^{kl}(\mathbf{r}) = \mathbf{V}_{oo}^{kl}(\mathbf{r}) + \xi_A \xi_C \mathbf{W}(\mathbf{r}), \quad \xi_{A,C} = \frac{\alpha_{A,C}}{a_0^3}$$

$$\mathbf{W}(\mathbf{r}) = \frac{1}{v_0} \int \int \int \mathbf{W}(\mathbf{q}) e^{-i\mathbf{q}\mathbf{r}\mathbf{d}\mathbf{q}}$$

$$\mathbf{W}(\mathbf{q}) = \sum [J_{\alpha\beta}^{\text{A}}(\mathbf{q}) J_{\alpha\beta}^{\text{C}}(\mathbf{q}) - (D_{\alpha\beta}^{\text{AC}}(\mathbf{q}))^2 \xi_A \xi_C]^{-1} \times \left\{ \sum [F_{\alpha n}^{\text{A}}(\omega_1, \mathbf{q}) F_{\beta m}^{\text{C}}(\omega_2, \mathbf{q}) + F_{\beta m}^{\text{A}}(\omega_2, \mathbf{q}) F_{\alpha n}^{\text{C}}(\omega_1, \mathbf{q})] D_{\alpha\beta}^{\text{AC}}(\mathbf{q}) - \frac{1}{\xi_C} F_{\alpha n}^{\text{A}}(\omega_1, \mathbf{q}) F_{\beta m}^{\text{A}}(\omega_2, \mathbf{q}) J_{\alpha\beta}^{\text{C}}(\mathbf{q}) - \frac{1}{\xi_A} F_{\alpha n}^{\text{A}}(\omega_1, \mathbf{q}) F_{\beta m}^{\text{C}}(\omega_2, \mathbf{q}) J_{\alpha\beta}^{\text{A}}(\mathbf{q}), J_{\alpha\beta}^{\text{A,C}} = E_{\alpha\beta} + \xi_{A,C} D_{\alpha\beta}^{\text{A,C}}(\mathbf{q}), \right. \quad (3)$$

where \mathbf{E} is the unit matrix; $\mathbf{D}^{\text{A}}(\mathbf{q})$, $\mathbf{D}^{\text{C}}(\mathbf{q})$, and $\mathbf{D}^{\text{AC}}(\mathbf{q})$ are the Fourier transforms of the intra- and interlattice dipole-dipole interaction matrices, and $\mathbf{F}^{\text{A,C}}(\omega_i, \mathbf{q})$ is the Fourier transform of the octupole-dipole interaction matrix.

The details of the calculation of the interaction matrices in Eq. (2) are presented in Ref. 6. Here we present only the computational results for Rb_2ZnCl_4 . In the present calculation we have used the following values of the unit-cell parameters of the hypothetical hexagonal phase of Rb_2ZnCl_4 : $a_0 = 7.3 \text{ \AA}$ and $c_0 = 10.58 \text{ \AA}$. The value of a_0 was determined by extrapolating the temperature dependence of this parameter in the paraelectric phase, and the value of c_0 was chosen by analogy with the oxide members of this family in which the hexagonal phase exists at high temperatures and a large jump in the parameter c_0 occurs at the transition into this phase.⁹

In calculating the octupole-dipole interaction, the interaction of the BX_4 tetrahedron with five and six nearest metals of type A and C, respectively, was taken into account. The dipole-dipole interaction was calculated by the Ewald method. The integration in \mathbf{q} -space was performed by the Gauss method. The polarizabilities were chosen so as to minimize the energy of the ferroelectric phase at low temperatures:

$$\alpha_A = 0.90 \text{ \AA}^3, \quad \alpha_C = 1.29 \text{ \AA}^3.$$

The octupole moment I_3 of the ZnCl_4 group was determined by matching the experimental value of the temperature of the paraelectric-to-incommensurate phase transition ($P \rightarrow I$) in Rb_2ZnCl_4 :

TABLE I. Effective interaction constants.

R	$V_{ij}^{\text{I,II}}(R), \text{ K}$			
	V_{11}	V_{12}	V_{13}	V_{14}
$\sqrt{a_0^2/3 + c_0^2/4}$	325.3	431.7	-746.1	-639.7
$\sqrt{4a_0^2/3 + c_0^2/4}$	99.8	52.8	135.8	88.8
$\sqrt{7a_0^2/3 + c_0^2/4}$	114.2	116.5	84.1	86.3
$\sqrt{13a_0^2/3 + c_0^2/4}$	-44.0	-23.0	-42.2	-21.1
$\sqrt{a_0^2/3 + 9c_0^2/4}$	116.2	92.4	17.9	-5.9
$\sqrt{16a_0^2/3 + c_0^2/4}$	-72.0	-44.4	-57.2	-29.6
$\sqrt{4a_0^2/3 + 9c_0^2/4}$	-11.9	2.4	-44.4	-30.1
$\sqrt{19a_0^2/3 + c_0^2/4}$	-25.8	-38.7	-5.2	-18.0
$\sqrt{7a_0^2/3 + 9c_0^2/4}$	-21.6	-29.5	-30.5	-38.4
$\sqrt{28a_0^2/3 + c_0^2/4}$	36.1	21.4	28.8	14.2

R	$V_{ij}^{\text{I,II}}(R) = V_{ij}^{\text{II,II}}(R), \text{ K}$			
	V_{11}	V_{12}	V_{13}	V_{14}
a_0	433.6	494.2	-249.1	-188.4
c_0	-72.7	-56.2	89.7	106.1
$a_0\sqrt{3}$	16.7	15.9	-6.9	-7.7
$\sqrt{a_0^2 + c_0^2}$	8.8	-7.5	52.9	36.6
$2a_0$	1.4	-0.3	-7.2	-8.9
$\sqrt{3a_0^2 + c_0^2}$	4.6	3.8	0.5	-0.3
$\sqrt{4a_0^2 + c_0^2}$	1.0	0.8	-0.3	-0.5
$a_0\sqrt{7}$	-4.4	-6.1	5.6	3.8
$2c_0$	17.6	14.7	-32.4	-35.3

$$I_3(\text{ZnCl}_4) = 83.58 \cdot 10^{-34} \text{ esu} \cdot \text{cm}^3.$$

The effective interaction constants $V_{ij}^{\text{I}}(R) = V_{ij}^{\text{II}}(R)$ and $V_{ij}^{\text{I,II}}(R)$ were calculated within twelve coordination spheres up to $R = 2c_0$ inclusively; the computed values are presented in Table I. As one can see from this table, the sign and magnitude of the interaction constants fluctuate as functions of the distance, so that there is a strong competition between the interactions. Note that the same competition between interactions also occurs in other crystals of the ACBX_4 family,^{6,10} but the interactions in Rb_2ZnCl_4 have a characteristic feature: Calculations of the energy at $T=0$ in a finite system ($16 \times 16 \times 24$) for phases with different types of uniform and nonuniform orderings show that several phases with close energies, including a ferroelectric phase observed below 190 K, are present in it. On the other hand, in CsLiSO_4 , for example, at low temperatures only two phases, including the experimentally observed phase, have a lower energy than other phases (see Table II). It is this peculiarity of the interactions in Rb_2ZnCl_4 that is apparently responsible for the presence of an incommensurate phase in it at finite temperatures.

TABLE II. Energies and structures of the ordered low-temperature phases.

Phase	Structures of the ordered phases						Energy, K	
	1	2	3	4	5	6	Rb ₂ ZnCl ₄	CsLiSO ₄
<i>a</i>	↑ ↓ ↓ ↑ ↓ ↑ ↑ ↓	↑ ↓ → ← ↓ ↑ ← →	← → → ← → ← ← →				-702	-534
<i>b</i>	← → ↓ ↑ ↑ ↓ → ←	↑ ↓ ↓ ↑ → ← ← →	← → → ← ↑ ↓ ↓ ↑				-410	-982
<i>c</i>	↑ ↓ ↓ ↑ ↑ ↓ ↓ ↑	↑ ↓ ↓ ↑ ↑ ↓ ↓ ↑	↑ ↓ ↓ ↑ ↑ ↓ ↓ ↑				-658	-598
<i>d</i>	← ← ↓ ↓ ← ← ↓ ↓	↑ ↑ ↓ ↓ ↑ ↑ ↓ ↓	← ← → → ← ← → →				-644	173
<i>e</i>	↑ ↑ ↓ ↓ ↑ ↑ ↓ ↓	↑ ↑ ↓ ↓ ↑ ↑ ↓ ↓	↑ ↑ ↓ ↓ ↑ ↑ ↓ ↓				-601	109
<i>f</i>	→ ↑ ← ↓ ↑ → ↓ ←	→ ↑ ← ↓ ↑ → ↓ ←	→ ↑ ← ↓ ↑ → ↓ ←				-556	-1052
<i>g</i>	1		2		3		-620	-244
	↑ ↑ ↓ ↓ ↓ ↓ ↑ ↑		↓ ↓ ↑ ↑ ↑ ↑ ↓ ↓		↑ ↑ ↓ ↓ ↓ ↓ ↑ ↑			
	4		5		6			
	↓ ↓ ↑ ↑ ↑ ↑ ↓ ↓		↑ ↑ ↓ ↓ ↓ ↓ ↑ ↑		↓ ↓ ↑ ↑ ↑ ↑ ↓ ↓			

3. COMPUTATIONAL METHOD

We employed the standard Monte Carlo method which is applied to Ising-type models.^{11,12} A modification was introduced in connection with the fact that in this case each BX₄ tetrahedron has four equally probable positions (instead of two as in the Ising model). The process of determining the thermodynamic quantities was initiated by setting the initial configuration of the system. The ordered configurations were usually chosen to initialize the Monte Carlo procedure at low temperatures. At the next step, when the temperature is increased, the last configuration at the preceding temperature was used as the initial configuration. Next, the program successively sorted through all pseudochanges in the lattice, examining each tetrahedron as an object for rotation into the new state. A random number generator was used to select one of the three possible states. The relative probability of two states¹² was examined

$$\rho_{\mu\nu} = \frac{\rho_\mu}{\rho_\nu} = \exp\left(-\frac{E_\mu - E_\nu}{kT}\right), \quad (4)$$

which describes the probability that a state ν with energy E_ν is engendered from a state μ with energy E_μ . If $\rho_{\mu\nu} > 1$ holds, the tetrahedron rotates. Otherwise the rotation of the tetrahedron is associated with a random number r , generated by the random number generator in the interval from 0 to 1. If $r < \rho_{\mu\nu}$ holds, the tetrahedron rotates.

Two types of boundary conditions were used: Periodic boundary conditions and boundary conditions with pseudospins (phantoms). The latter conditions were recently pro-

posed in Ref. 13 for investigating systems with competing interactions. In Ref. 13 the two-dimensional triangular X - Y model was studied by the Monte Carlo method. In the present work the boundary conditions with phantoms are somewhat modified from those of Ref. 13, since here a discrete pseudospin, rather than the continuous pseudospin of the X - Y model, is present at each lattice site. The changes concerned the configuration of the phantom spins surrounding the main spins. The number of phantom spins is determined by the number of interacting coordination spheres, and their configuration after each Monte Carlo step was set according to the obtained configuration of the main lattice.

It should be noted that we tried free boundary conditions, but in the present case, even at low temperatures, the system very rapidly slid into a metastable state and remained in it with a reasonable number of Monte Carlo steps. This is associated with the fact that, even for quite large lattices, too many "spins" remain free because of the large number of interactions, and the competition between them makes the system very unstable.

The calculations were performed on $12 \times 12 \times 24$ and $16 \times 16 \times 24$ three-dimensional hexagonal lattices. The thermodynamic quantities were calculated in the standard manner:^{11,12}

$$U = \sum_{m=1}^{n \times n \times n_1} \sum_{s=1}^{19} V_{ij}(s, m), \quad C = \frac{N^2}{kT^2} (\Delta U)^2, \quad (5)$$

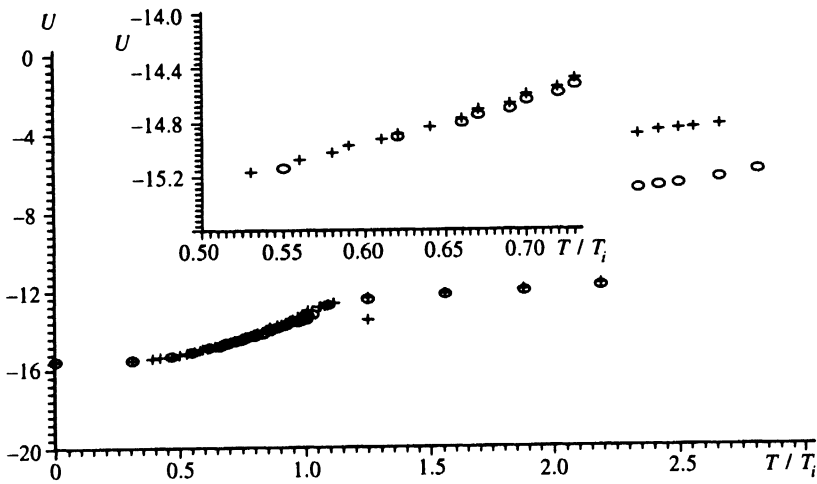


FIG. 3. Temperature dependence of the internal energy: The crosses and ellipses represent boundary conditions with phantom spins and periodic boundary conditions, respectively.

$$\chi_i = \frac{N^2}{kT} (\Delta \eta_i)^2,$$

where U is the internal energy, $V_{ij}(s, m)$ is defined in Eq. (2), s is the number of the coordination sphere, m is the lattice site, C is the specific heat, η_i are the order parameters (which will be defined below), χ_i is the susceptibility, and $(\Delta A)^2 = \langle A^2 \rangle - \langle A \rangle^2$. One Monte Carlo step consisted of successive attempts to rotate all tetrahedra. The first 1000 Monte Carlo steps were discarded and did not participate in the averaging. The averages were calculated in two steps: after p steps the average over a group (usually $p = 50$) was determined and then the final averaging over groups (usually 70) was performed. All calculations were then repeated at a different temperature.

4. RESULTS

At low temperatures the structure of the ordered phase which the system reaches as a result of the Monte Carlo calculations has the following occupation numbers:

$$\begin{aligned} n_1^I(R_0) = n_3^I(R_1) = n_1^{II}(R_2) = n_3^{II}(R_3) = 1, \\ n_1^I(R_4) = n_3^I(R_5) = n_2^{II}(R_6) = n_4^{II}(R_7) = 1, \\ n_2^I(R_8) = n_4^I(R_9) = n_2^{II}(R_{10}) = n_4^{II}(R_{11}) = 1, \end{aligned} \quad (6)$$

where

$$\begin{aligned} R_0 = 0, \quad R_1 = a_0, \\ R_2 = \sqrt{4a_0^2/3 + c_0^2/4}, \quad R_3 = \sqrt{a_0^2/3 + c_0^2/4}, \\ R_4 = c_0, \quad R_5 = \sqrt{a_0^2 + c_0^2}, \\ R_6 = \sqrt{a_0^2/3 + 9c_0^2/4}, \quad R_7 = \sqrt{4a_0^2/3 + 9c_0^2/4}, \\ R_8 = 2c_0, \quad R_9 = \sqrt{a_0^2 + 4c_0^2}, \\ R_{10} = \sqrt{a_0^2/3 + 25c_0^2/4}, \quad R_{11} = \sqrt{ra_0^2/3 + 25c_0^2/4}. \end{aligned}$$

The values of $n_i^k(R)$ were determined from the Monte Carlo data at the temperature $T/T_i = 0.3$, where T_i is the temperature of the transition into the modulated phase. At lower temperatures the problem of metastable states arises when the system cools from the disordered or modulated

phases. The ordered phase has orthorhombic symmetry with the space group C_{2v}^9 and 12 molecules per unit cell.

In the Monte Carlo procedure the order parameters were calculated as follows:

$$\begin{aligned} \eta_1 = \frac{1}{4} [n_1^I(R_0) + n_2^I(R_0) - n_3^I(R_0) - n_4^I(R_0) \\ + n_3^I(R_1) + n_4^I(R_1) - n_1^I(R_1) - n_2^I(R_2) \\ + n_3^{II}(R_3) + n_4^{II}(R_3) - n_1^{II}(R_3) - n_2^{II}(R_3) \\ + n_1^{II}(R_2) + n_2^{II}(R_2) - n_3^{II}(R_2) - n_4^{II}(R_2)], \end{aligned} \quad (7)$$

$$\begin{aligned} \eta_2 = \frac{1}{12} \left\{ \sum_{R=R_0, R_1, R_4, R_5} [n_1^I(R) - n_2^I(R) + n_3^I(R) - n_4^I(R)] \right. \\ + \sum_{R=R_2, R_3} [n_1^{II}(R) - n_2^{II}(R) + n_3^{II}(R) - n_4^{II}(R)] \\ + \sum_{R=R_8, R_9} [n_2^I(R) - n_1^I(R) + n_4^I(R) - n_3^I(R)] \\ \left. + \sum_{R=R_6, R_7, R_{10}, R_{11}} [n_2^{II}(R) - n_1^{II}(R) + n_4^{II}(R) - n_3^{II}(R)] \right\}, \end{aligned} \quad (8)$$

where the equivalence of the cell parameters a_0 and b_0 of the hexagonal phase is taken into account.

The computational results for the phase diagram and the behavior of the thermodynamic quantities for Rb_2ZnCl_4 are displayed in Figs. 3–7. We do not present the computational results here for the $12 \times 12 \times 24$ lattice, since they are essentially identical to the computational results for the $16 \times 16 \times 24$ lattice (excluding the behavior of the specific heat inside the incommensurate phase), and in what follows we discuss only the computational results for the $16 \times 16 \times 24$ lattice. Here, three successive phase transitions occur. The first transition, occurring with decreasing temperature, from the completely disordered hexagonal phase into an orthorhombic phase is associated with partial ordering of the ZnCl_4 tetrahedra, which in this phase take on with equal probability predominantly two of four positions. The symmetry of this phase is D_{2h}^{16} and the unit cell contains four

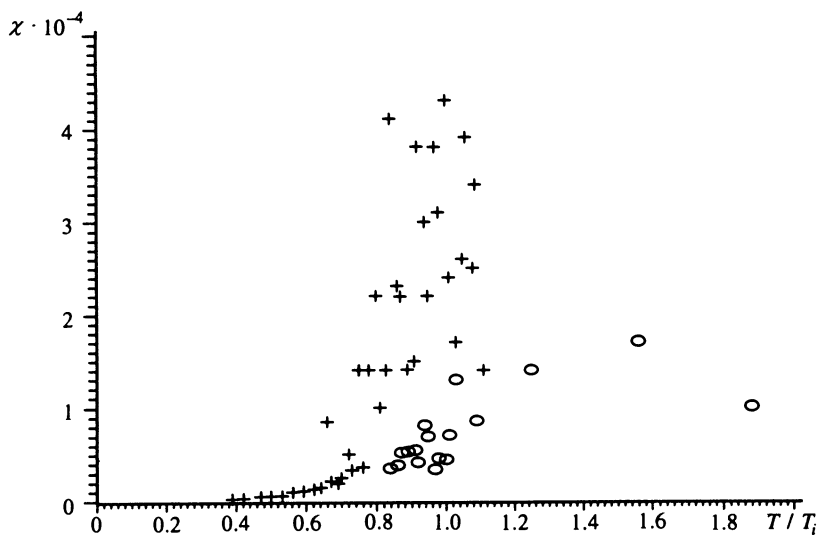


FIG. 4. Temperature dependence of the susceptibility χ_2 . The notation is the same as in Fig. 3.

molecules; cell doubling (relative to the hexagonal phase) occurs in a plane perpendicular to the hexagonal axis. It is this structure that is observed Rb_2ZnCl_4 at high temperatures.¹⁻³ The computed temperature of the transition from the hexagonal into the orthorhombic phase $T_{c1} \approx 700$ K is much higher than the decomposition temperature ($T = 550$ K). For this reason this transition is not observed in Rb_2ZnCl_4 .

As the temperature decreases further, a phase transition into the modulated phase occurs at $T_i = T_i^{\text{exp}} = 302$ K. Finally,

at $T_{c2} \approx 200$ K a lock-in transition into a ferroelectric ordered phase with the space group C_{2v}^9 and twelve molecules per unit cell occurs. The pseudohexagonal axis is tripled compared to the paraelectric phase, as is observed experimentally.¹ The calculated temperature of the *lock-in* transition agrees well with the experimental value $T_{c2}^{\text{exp}} = 192$ K. The temperatures of the hexagonal \rightarrow orthorhombic and orthorhombic \rightarrow incommensurate phase transitions were determined from the Monte Carlo data according to the peaks in the temperature dependence of the specific

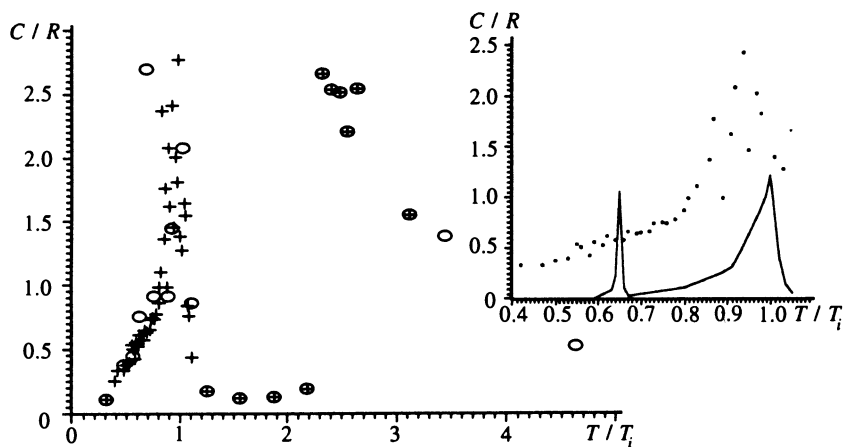


FIG. 5. Temperature dependence of the specific heat (same notation as in Fig. 3); R is the gas constant. Inset: Comparison of the Monte Carlo data (dots, boundary conditions with phantom spins) with the experimental data of Ref. 14 (solid trace).

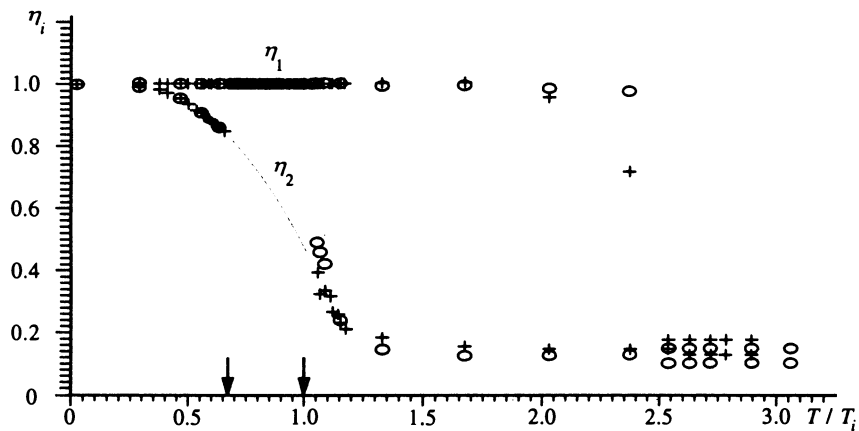


FIG. 6. Temperature dependence of the order parameters. Same notation as in Fig. 3.

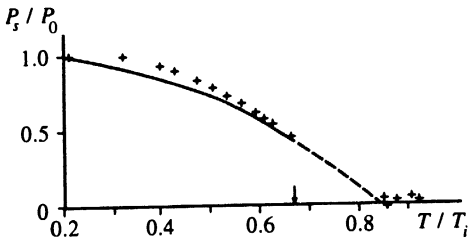


FIG. 7. Temperature dependence of the spontaneous polarization: The crosses represent the Monte Carlo data (phantom-spin boundary conditions) and the dashed curve represents the average (over layers) value of P_s in the modulated phase. The solid curve represents the experimental data of Ref. 15.

heat (Fig. 5). We encountered definite difficulties in determining the temperature of the lock-in transition, since there is a large spread in the specific-heat data for the incommensurate phase (Fig. 5). This spread does not decrease significantly as the lattice size increases. We estimated the temperature of the *lock-in* transition from the inflection in the temperature dependence of the internal energy (Fig. 3).

We now discuss the incommensurate phase. The structure of this phase is spatially modulated along the pseudo-hexagonal axis and the modulation depends on the temperature. According to the Monte Carlo data, the ordering of the BX_4 tetrahedra in layers perpendicular to the hexagonal phase is uniform at all temperatures, including the region in which the modulated phase exists. Inside this phase, however, the degree of ordering of the tetrahedra changes from layer to layer. Figure 8 displays the degree of ordering of the tetrahedra in the layers for two temperatures in the modulated phase. The ordering in the layers in the ordered ferroelectric phase is shown for comparison in Fig. 8b. Here only the computational results for the case of boundary conditions with phantom spins are presented. The same results are obtained for periodic boundary conditions. The long-wavelength modulation inside the incommensurate phase depends on the temperature. This is especially noticeable when phantom spins are used in the boundary conditions, when the system itself selects the modulation period. At all temperatures the periodic boundary conditions impose a specific period on the system. One can see from Fig. 8 that inside the incommensurate phase short-wavelength modulation of the ordering of the layers is present in addition to long-wavelength modulation. The period of this modulation is c_0 , i.e., where c_0 is the cell parameter of the ferroelectric phase, and here, together with different orientations of the tetrahedra in the layers, there is a large difference in the average magnitude of these orientations from layer to layer inside the tripled cell. Note that traces of this modulation are present in both the ferroelectric and paraelectric phases at temperatures close to the modulated-phase region.

To determine the temperature dependence of the modulation periods, we calculated the structure factor $S(\mathbf{q})$ in terms of the correlation function $G_{11}(\mathbf{R})$:

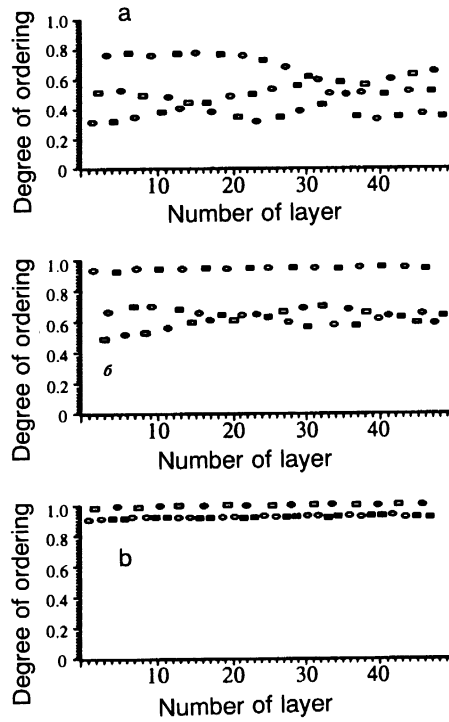


FIG. 8. Spatial dependence of the degree of ordering of the layers at different temperatures $T=255$ K (a), 225 K (b), and 135 K (c). Phantom-spin boundary conditions; the notation corresponds to the configurations from Table II: open circles — a_1 ; filled ellipses — a_4 ; open ellipses — a_2 ; filled ellipses — a_5 .

$$S(\mathbf{q}) = \sum_{\mathbf{R}} G_{11}(\mathbf{R}) e^{i\mathbf{q}\mathbf{R}}, \quad (9)$$

$$G_{11}(\mathbf{R}) = \sum_{i=1}^{n \times n \times n_1} C_1(\mathbf{r}_i) C_1(\mathbf{r}_i - \mathbf{R}).$$

The functions $S(0,0,q)$ and $S(2,0,q)$ for different temperatures are displayed in Fig. 9. One can see that in the ferroelectric phase, in addition to the peak at $q=0$, there is a peak at $q=1/3$. We note that the same peak also appears at all values of q which are multiples of $1/3$. Inside the modulated phase the position of this peak varies very little with temperature, but the intensity of the peak decreases strongly with increasing temperature and the peak vanishes in the paraelectric phase.

5. DISCUSSION. COMPARISON WITH EXPERIMENT

The temperature dependence of the internal energy, specific heat, order parameters, and susceptibility, as obtained from the Monte Carlo data for two types of boundary conditions, is displayed in Figs. 3-6. The solid trace in the inset of Fig. 5 represents the experimental curve of the specific heat of Rb_2ZnCl_4 . As one can see from this figure, the agreement between the computed and experimental curves is satisfactory, including the region in which the modulated phase exists, where the Monte Carlo calculations give a large spread in the specific heat, as has already been mentioned. Crystalline Rb_2ZnCl_4 is a nonintrinsic ferroelectric material and the

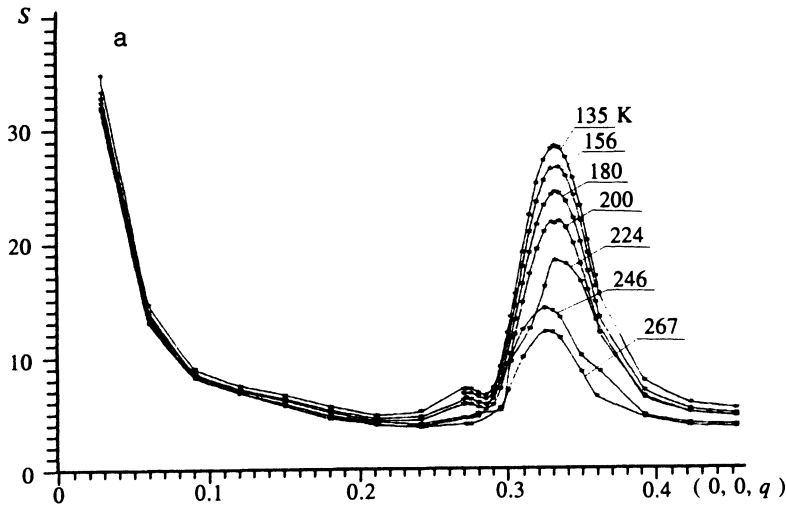
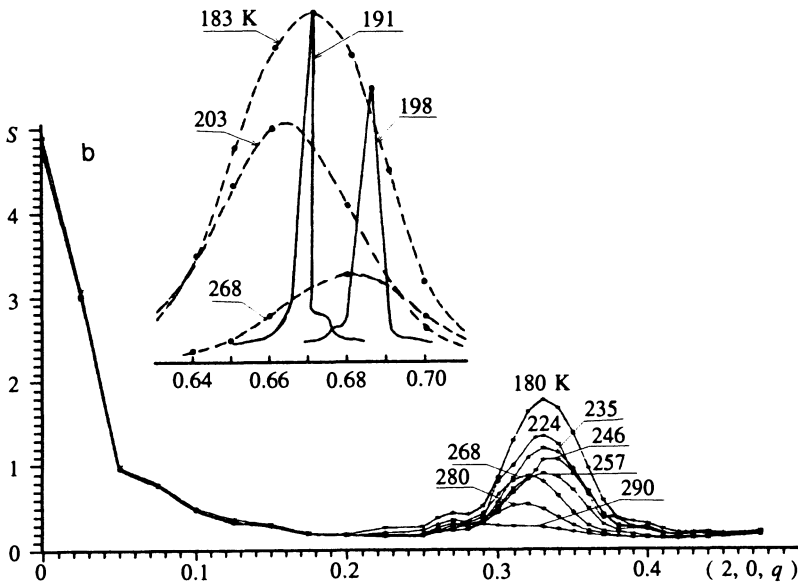


FIG. 9. Structure factor as a function of the wave vector at different temperatures. Inset: Profile of the x-ray reflection of the first satellite with $q=(2,0,2/3+\delta)$ in Rb_2ZnCl_4 . The dashed curves represent the Monte Carlo data (phantom-spin boundary conditions) and the solid curves represent the experimental data.¹⁶



measured quantity is the spontaneous polarization P_s . In this model the absolute value of the polarization in the ferroelectric phase is not calculated, since displacements of metal atoms and distortions of the BX_4 tetrahedra in the low-symmetry phase are not studied in this model, but the temperature dependence of P_s can be obtained. The quantity P_s , defined by the equations

$$P_s = \frac{1}{4} [n_1^I(R_0) - n_2^I(R_0) + n_3^I(R_0) - n_4^I(R_0) + n_1^{II}(R_3) - n_2^{II}(R_3) + n_3^{II}(R_3) - n_4^{II}(R_3) + n_2^I(R_1) - n_1^I(R_1) + n_4^I(R_1) - n_3^I(R_1) + n_2^{II}(R_2) - n_1^{II}(R_2) + n_4^{II}(R_2) - n_3^{II}(R_2)],$$

is proportional to the spontaneous polarization. Figure 7 displays both the computed and experimental temperature dependence of P_s . The agreement between these curves is good.

The structure of the modulated phase of Rb_2ZnCl_4 was determined in Ref. 17. It was found that the modulation of

the structure is determined mainly by the nonuniform (in the direction of the pseudohexagonal axis) rotation of the $ZnCl_4$ tetrahedra, and it has a long-wavelength character. The short-wavelength modulation of the structure found here as a result of the Monte Carlo calculations in the temperature range $200\text{ K} < T < 300\text{ K}$ was not observed in experiments. The computed long-wavelength modulation of the structure agrees qualitatively with the experimental modulation.

The temperature dependence of the modulation vector in the incommensurate phase of Rb_2ZnCl_4 was studied in Ref. 16 in connection with the temperature dependence of the x-ray reflections on the vectors $(2,0,q)$. The inset in Fig. 9 displays the experimental and Monte Carlo values of the intensities at different temperatures inside the modulated phase, and Fig. 10 displays the temperature dependence of δ . As one can see from these figures, the agreement between the computed and experimental curves is only qualitative. The experimental curve of the intensity is much narrower than the computed curve, and the measured maximum value

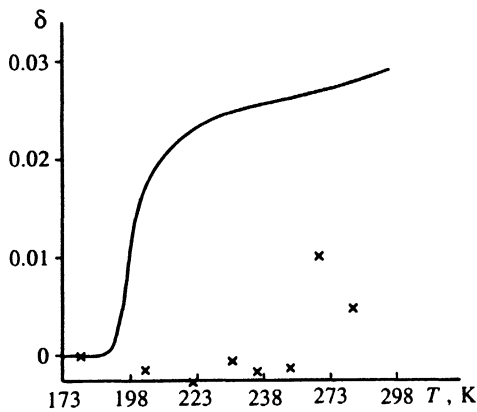


FIG. 10. Temperature dependence of the modulation vector $\mathbf{q}=(1-\delta)\mathbf{c}^*/3$ in Rb_2ZnCl_4 . The crosses represent the Monte Carlo data (phantom-spin boundary conditions) and the solid curve represents the experimental data of Ref. 16.

of δ is almost three times the maximum value extracted from the Monte Carlo data.

As mentioned in the introduction, at 74 K Rb_2ZnCl_4 undergoes another transition into a monoclinic phase, whose structure has not yet been determined experimentally. In Ref. 4 a structure with the space group $C1c1$ and 48 molecules per unit cell (phase *b* in Table II) was obtained for this phase by the method of molecular dynamics with the inter- and intramolecular interaction constants calculated from first principles. The Monte Carlo method does not work at low temperatures, and in the present work the transition into the monoclinic phase was not investigated. As one can see from Table II, however, the energy of the phase calculated at $T=0$ for a finite lattice with the constants given in Table I and in Ref. 4 is much higher than the energy of several phases with other types of ordering of the ZnCl_4 tetrahedra, and it is unlikely that this phase is realized in Rb_2ZnCl_4 at low temperatures.

In conclusion, we shall summarize the basic results obtained in this work. The model with the interaction constants (calculated in the electrostatic approximation) between the ZnCl_4 tetrahedra describes correctly the sequence of transitions in Rb_2ZnCl_4 , including the intermediate modulated phase. The computed temperatures of the *lock-in* transition into the commensurate ferroelectric phase and the behavior of the thermodynamic quantities agree satisfactorily with the experimental data. One possible prediction of this work is the existence, in the modulated phase, of a short-wavelength

modulation associated not only with different orientations of the tetrahedra but also with the substantially different degree of ordering of the tetrahedra in layers belonging to a unit cell of the ferroelectric phase. Another prediction concerns the change in the phase diagram of Rb_2ZnCl_4 under uniaxial pressure. We investigated the change accompanying a change in the ratio c_0/a_0 of the cell parameters of the hexagonal phase in the region where the modulated phase exists. We found that this region decreases sharply as a result of a small decrease in the parameter c_0 and vanishes together with the tripled ferroelectric phase as the ratio c_0/a_0 decreases by approximately 10%. This means that the phase diagram of Rb_2ZnCl_4 80 state will change substantially under uniaxial pressure applied along the pseudohexagonal axis. It would be interesting to check these predictions experimentally and to determine the structure of the low-temperature phase.

We thank the Russian Fund for Fundamental Research (Project 93-022425) and the Krasnoyarsk Regional Science Fund (Grant 2F0038) for financial support.

¹ K. S. Aleksandrov and B. V. Beznosikov, *Structural Phase Transitions in Crystals (Potassium Selenate Family)* [in Russian], Nauka, Novosibirsk, 1993.

² H. Z. Cummins, *Phys. Rep.* **185**, 211 (1990).

³ W. Eysel, *Strukturen und Kristallochemische Verwandtschaft bei Verbindungen $A(BX)$ und $A_2(BX_3)$* , Dissertation, Aachen University, 1975.

⁴ H. M. Lu and I. R. Hardy, *Phys. Rev.* **B 42**, 8339 (1992).

⁵ V. I. Zinenko and D. Kh. Blat, *Fiz. Tverd. Tela (Leningrad)* **20**, 3539 (1978) [*Sov. Phys. Solid State* **20**, 2047 (1978)].

⁶ N. G. Zamkova and V. I. Zinenko, *Fiz. Tverd. Tela (Leningrad)* **34**, 2735 (1992) [*Sov. Phys. Solid State* **34**, 1464 (1992)].

⁷ H. M. James and T. A. Keenan, *J. Chem. Phys.* **31**, 12 (1959).

⁸ V. G. Vaks, *Introduction to the Microscopic Theory of Ferroelectric Materials* [in Russian], Nauka, Moscow, 1973.

⁹ M. Miyake, H. Morikawa, and I. Shin-ichi, *Acta Crystallog.* **B 36**, 532 (1980).

¹⁰ N. G. Zamkova and V. I. Zinenko, *J. Phys. Condensed Matter* **6**, 9043 (1994).

¹¹ K. Binder in *Monte Carlo Methods in Statistical Physics*, edited by K. Binder, Springer-Verlag, N. Y., 1979.

¹² D. P. Landau, *Phys. Rev.* **13**, 2997 (1976).

¹³ W. M. Saslow, M. Gabay, and W. M. Zhang, *Phys. Rev. Lett.* **68**, 3627 (1992).

¹⁴ K. Nomoto, T. Atake, B. K. Chaudhuri, and H. Chihara, *J. Phys. Soc. Jpn.* **52**, 3475 (1983).

¹⁵ K. Hamano, Y. Ikeda, T. Fujimoto, K. Ema, and S. Hirotsu, *J. Phys. Soc. Jpn.* **49**, 2278 (1980).

¹⁶ H. Mashiyama, S. Tanisaki, and K. Hamano, *J. Phys. Soc. Jpn.* **51**, 2538 (1982).

¹⁷ K. Iton, A. Hinasada, M. Daiki, and E. Nakamya, *J. Phys. Soc. Jpn.* **58**, 2070 (1989).

Translated by M. E. Alferieff